Light: Science & Applications (2016) 5, e16130; doi:10.1038/lsa.2016.130
Official journal of the CIOMP 2047-7538/16
www.nature.com/lsa

ORIGINAL ARTICLE

Plasma-induced, nitrogen-doped graphene-based aerogels for high-performance supercapacitors

Xue-Yu Zhang[1], Shi-Han Sun[1], Xiao-Juan Sun[2], Yan-Rong Zhao[1], Li Chen[3], Yue Yang[1], Wei Lü[1] and Da-Bing Li[2]

Commonly used energy storage devices include stacked layers of active materials on two-dimensional sheets, and the limited specific surface area restricts the further development of energy storage. Three-dimensional (3D) structures with high specific surface areas would improve device performance. Herein, we present a novel procedure to fabricate macroscopic, high-quality, nitrogen-doped, 3D graphene/nanoparticle aerogels. The procedure includes vacuum filtration, freeze-drying, and plasma treatment, which can be further expanded for large-scale production of nitrogen-doped, graphene-based aerogels. The behavior of the supercapacitor is investigated using a typical nitrogen-doped graphene/Fe_3O_4 nanoparticle 3D structure (NG/Fe_3O_4). Compared with 3D graphene/Fe_3O_4 structures prepared by the traditional hydrothermal method, the NG/Fe_3O_4 supercapacitor prepared by the present method has a 153% improvement in specific capacitance, and there is no obvious decrease in specific capacitance after 1000 cycles. The present work provides a new and facile method to produce large-scale, 3D, graphene-based materials with high specific capacitance for energy storage.

Light: Science & Applications (2016) **5,** e16130; doi:10.1038/lsa.2016.130; published online 7 October 2016

Keywords: energy storage; N-doping; plasma; three-dimension

INTRODUCTION

The intrinsic two-dimensional (2D) structure of graphene provides unique physical properties, making it possible to fabricate self-assembled, three-dimensional (3D) architectures[1–13]. Combining functional nanomaterials with 3D graphene structures would enhance their specific applications. Recently, 3D, graphene-based materials have attracted attention due to their porous structure, which provides a high specific surface area and synergistic effects in the composites[14–19]. The 3D, graphene-based hybrids are becoming candidates for energy storage, such as in Li ion batteries, hydrogen storage and supercapacitors[20–24]. Several methods have been reported for fabricating 3D, porous, graphene-based structures, including chemical vapor deposition[25], growth assisted by a template[26–28] and chemical self-assembly[29–34]. In spite of the significant development for constructing 3D graphene-based structures, these commonly used fabrication methods are generally multistep, hard to control and involve harmful chemical agents. Therefore, further development for preparing high-quality 3D structures is still highly desirable.

In addition, the capacitance of intrinsic graphene is not sufficient for commercial applications but can be improved by N-doping[35-39]. The preparation of N-doped graphene sheets by arc discharge/plasma treatment and chemical vapor deposition (CVD) thermal annealing of graphene oxide (GO) with NH_3 have been reported[35,40,41]. Plasma treatment is an eco-friendly and efficient way to produce N-doped graphene sheets, and several reports have demonstrated N-doping of graphene by plasma[42,43]. However, these reports address 2D structures and are not aimed at energy storage. A method for fabricating high-quality, N-doped, graphene-based, hybrid, 3D structures does not exist.

In this work, we report a novel method for preparing N-doped, 3D, graphene/Fe_3O_4, nanoparticle aerogel (NG/Fe_3O_4), which can be expanded for large-scale production of nitrogen-doped, graphene-based aerogel and various active nanomaterials can be incorporated into the 3D hybrid structures. The high-quality NG/Fe_3O_4 aerogels are acquired by controllable physical treatment of GO. Compared with the 3D reduced-graphene/Fe_3O_4 (RGO/Fe_3O_4) prepared by the commonly used hydrothermal method, the present method produces greatly improved porous networks and exhibits significantly enhanced supercapacitor performance. The present work provides a new and facile method to produce high-quality, 3D, graphene-based materials for application in energy storage.

MATERIALS AND METHODS

Preparation of GO and Fe_3O_4 nanoparticles

A modified Hummers method was used to prepare GO. Fe_3O_4 nanoparticles (NPs) were prepared by $FeCl_3{\cdot}6H_2O$ (58 mg) and $FeCl_2{\cdot}4H_2O$ (21.5 mg), which were added to 30 ml deionized water and deoxygenated for 15 min with nitrogen gas. After heating

[1]Key Laboratory of Advanced Structural Materials, Ministry of Education & Advanced Institute of Materials Science, Changchun University of Technology, Changchun 130012, China; [2]State Key Laboratory of Luminescence and Applications, Changchun Institute of Optics, Fine Mechanics and Physics, Chinese Academy of Sciences, Changchun 130033, China and [3]School of Basic Sciences & Advanced Institute of Materials Science, Changchun University of Technology, Changchun 130012, China
Correspondence: DB Li, Email: lidb@ciomp.ac.cn; W Lü, Email: lw771119@hotmail.com
Received 26 January 2016; revised 6 March 2016; accepted 7 March 2016; accepted article preview online 8 March 2016

to 80 °C, $N_2H_4 \cdot H_2O$ (600 μl, 20 wt%) was injected rapidly and kept stirring for 1 h. The resulting Fe_3O_4 NPs were separated from the reaction mixture with a magnet after cooling to room temperature.

Preparation of NG/Fe_3O_4

A GO solution, including appropriate Fe_3O_4 NPs, was stirred for 1 h to obtain the GO/Fe_3O_4 suspension. Then, the GO/Fe_3O_4 suspension was deposited onto Ni-foam by vacuum filtration, followed by freeze-drying. Finally, the GO/Fe_3O_4 composites were reduced and nitrogen-doped simultaneously by hollow cathode (HCD) plasma discharge for 15 min in Ar and N_2 (Figure 1). The as-prepared sample was denoted as NG/Fe_3O_4. A schematic view of the HCD system used for the plasma treatment and the plasma experiment parameters are shown in Supplementary Fig. S1 and Table SI, respectively.

Hydrothermal synthesis of RGO/Fe_3O_4

For comparison, RGO/Fe_3O_4 fabricated by the commonly used hydrothermal method was prepared, and the electrochemical behavior was investigated. The GO/Fe_3O_4 suspension was kept in an autoclave at 180 °C for 12 h, followed by freeze-drying. A paste, including the active materials (RGO/Fe_3O_4), conductive carbon black and polyvinylidene fluoride, was used to prepare test electrodes on Ni-foam.

Characterization and electrochemical measurements

X-ray diffraction (XRD) measurements were performed with CuKa radiation (D-MAX II A, $\lambda = 0.15406$ nm). A VG ESCALAB MKII (Thermo Scientific, Waltham, MA, USA) was used for the X-ray photoelectron spectroscopy (XPS) investigation. Transmission electron microscopy (TEM) images were acquired by a JEOL2010 (JEOL, Tokyo, Japan). Fourier transform infrared spectroscopy (FTIR) curves were obtained on a VERTEX 70 (Bruker, Ettlingen, Germany). The electrical conductivity of NG/Fe_3O_4 and RGO/Fe_3O_4 aerogel samples was determined via the four-probe method at room temperature. An IVIUMSTAT (Ivium, Eindhoven, Netherlands) electrochemical workstation was used for the electrochemical investigations, and the electrolyte was 6 M KOH. The galvanostatic charge – discharge was measured under different current densities between − 1.0 and 0 V. The cyclic voltammetry (CV) was measured at different scan rates (5, 20, 100 and 200 V s^{-1}) between − 1.0 and 0 V. The electrochemical impedance spectroscopy was acquired from 100 kHz to 0.01 Hz by applying a signal of 14.14 mV.

RESULTS AND DISCUSSION

Figure 1 shows the experimental procedures of the hydrothermal synthesis of NG/Fe_3O_4. The GO/Fe_3O_4 mixed suspension was deposited onto Ni-foam by vacuum filtration, followed by freeze-drying. Finally, the GO/Fe_3O_4 composites were reduced and nitrogen-doped simultaneously by plasma treatment. Using the hydrothermal method, a gel-like cylinder of RGO/Fe_3O_4 was constructed, as shown in Figure 2a. The formation of a 3D porous network with micrometer-sized pores was confirmed by scanning electron microscopy (SEM), as shown in Figure 2b and 2c. However, as in the commonly used hydrothermal methods, the aggregation of graphene sheets during hydrogel formation was inevitable due to the reduction-induced strong π-stacking interaction between graphene sheets, which is originally prohibited by the oxygen-containing surface groups of GO. The network walls of RGO/Fe_3O_4 show a tendency of layered aggregation, even though the decoration of Fe_3O_4 NPs as spacers on graphene nanosheets partially prevents the aggregation. Compared with hydrothermally prepared RGO/Fe_3O_4, NG/Fe_3O_4 exhibits greatly improved 3D architectures. The SEM image of NG/Fe_3O_4 (Figure 2d) is highly transparent, and the bone of the Ni-foam could be observed clearly. The 3D porous networks are directly formed on the bone by vacuum filtration and freeze-drying. Figure 2e and 2f shows that very thin graphene sheets make up the walls of NG/Fe_3O_4. The average size of the pores is several tens of microns, which is larger than that of RGO/Fe_3O_4.

For RGO/Fe_3O_4 nanostructures, a paste including RGO/Fe_3O_4, conductive carbon black and polyvinylidene fluoride was used to prepare test electrodes on Ni-foam. For comparison, a Ni-foam electrode decorated by RGO/Fe_3O_4 was directly prepared by the hydrothermal process without further addition of conductive carbon black and polyvinylidene fluoride, as follows: a Ni-foam electrode was soaked in the GO/Fe_3O_4 suspension and kept in an autoclave at 180 °C for 12 h, followed by freeze-drying, which resulted in the formation of an RGO/Fe_3O_4-decorated, Ni-foam electrode (RGO/Fe_3O_4@ Ni-foam) produced by the hydrothermal process, as shown in Supplementary Fig. S2c. The microstructure of the RGO/Fe_3O_4@ Ni-foam was similar to that of the RGO/Fe_3O_4, as shown in Figure 2a-2c. In addition, Supplementary Fig. S2d and S2e reveals that the scrolled 3D structures are covered on the Ni bones and have similar morphology to that of RGO/Fe_3O_4, and the aggregation of graphene sheets during hydrogel formation was observed. This result indicates that the preparation method of the aerogel plays a key role in avoiding the aggregation tendency in the reduction process. The larger pore sizes and thinner pore walls increased the specific surface area of NG/Fe_3O_4 (92 m^2 g^{-1}) compared to that of RGO/Fe_3O_4 (55 m^2 g^{-1}) based on the BET results (Supplementary Fig. S3). These properties of NG/Fe_3O_4 are directly related to the potential applications from adsorbents to supercapacitors.

Both samples had similar TEM images, and the nanosized Fe_3O_4 particles were anchored on graphene uniformly, suggesting efficient assembly between the graphene sheets and the NPs (Supplementary Fig. S4 and Figure 2g). In this work, the diameters of the Fe_3O_4 particles were in the range of 10 – 15 nm. The density and size of the Fe_3O_4 particles in the NG/Fe_3O_4 and RGO/Fe_3O_4 samples were almost identical. Figure 2h shows the XRD curves of Fe_3O_4, NG/Fe_3O_4 and RGO/Fe_3O_4. For all three samples, the main diffraction peaks were assigned to (111), (311), (220), (422), (440), (400) and (511) of the crystal planes of Fe_3O_4, consistent with the Fe_3O_4 JCPDS card, which suggests that the chemical constitution of Fe_3O_4 was retained after the hydrothermal synthesis and plasma treatment. The sharp diffraction peak at 10.3° in GO, as shown in Supplementary Fig. S5, was replaced by a broad peak between 20° and 30°, which results from the (002) reflection of the graphene of NG/Fe_3O_4 and RGO/Fe_3O_4, indicating that GO was reduced by the hydrothermal and plasma treatment.

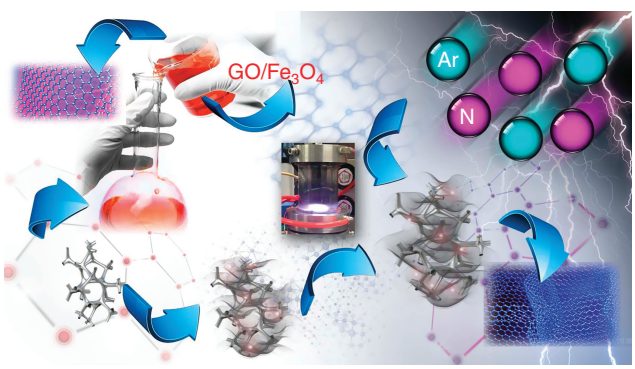

Figure 1 Schematic illustration of the synthetic procedures for NG/Fe_3O_4.

doi:10.1038/lsa.2016.130

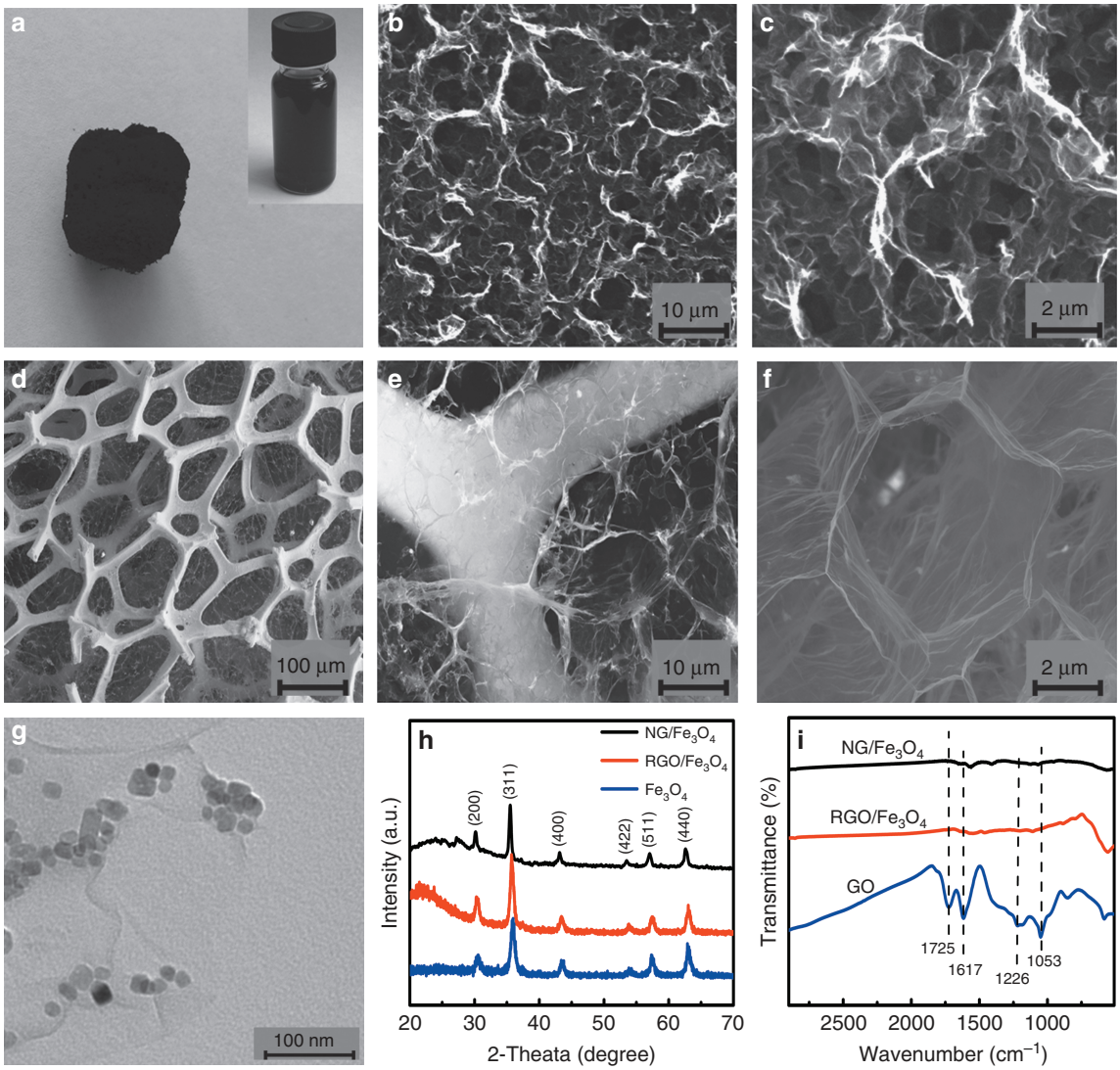

Figure 2 SEM images of RGO/Fe_3O_4 and NG/Fe_3O_4: (**a**) photograph of hydrothermal 3D RGO/Fe_3O_4; (**b**, **c**) SEM images of 3D RGO/Fe_3O_4 prepared by the hydrothermal process; (**d–f**) SEM images of 3D NG/Fe_3O_4 with different magnifications. (**g**) TEM images of NG/Fe_3O_4. (**h**) XRD picture of the as-prepared Fe_3O_4, NG/Fe_3O_4 and RGO/Fe_3O_4. (**i**) FTIR spectra of GO, NG/Fe_3O_4 and RGO/Fe_3O_4.

Figure 2i summarizes the FTIR spectra of GO, NG/Fe_3O_4 and RGO/Fe_3O_4. GO exhibits typical oxygen-related functional groups. The peaks at 1053 and 1226 cm^{-1} are attributed to the C – O and phenolic C – OH vibrations, whereas that of 1725 cm^{-1} is originated from the C = O vibration[44–46]. For RGO/Fe_3O_4 and NG/Fe_3O_4, an Fe–O related peak at 570 cm^{-1} was observed[47], which indicates a C–O–Fe linkage between the graphene nanosheets and the Fe_3O_4 NPs.

The XPS surveys of GO/Fe_3O_4, RGO/Fe_3O_4 and NG/Fe_3O_4 are shown in Figure 3a. For all three samples, peaks corresponding to the C 1s and O 1s were observed. Compared with GO/Fe_3O_4, the O 1s peak intensities of RGO/Fe_3O_4 and NG/Fe_3O_4 decreased, suggesting an increased C/O ratio after reduction by the hydrothermal process and plasma treatment, and the oxygen-related functional groups were efficiently removed. This hypothesis was confirmed by the deconvoluted C 1s spectra (Figure 3b). The weak signals of C-O and C = O in RGO/Fe_3O_4 compared with that of GO/Fe_3O_4 suggest that most of the GO was reduced, and the residual oxygen-related functional groups resulted from the incomplete reduction during the hydrothermal process. However, the oxygen-related peaks in the NG/Fe_3O_4 were nearly invisible, which indicates that the plasma treatment was more efficient for the reduction of 3D GO-based hybrids than the hydrothermal method. The formation of Fe_3O_4 in RGO/Fe_3O_4 and NG/Fe_3O_4 was further confirmed by the Fe 2p spectra (Figure 3c). Two characteristic peaks corresponding to Fe $2p_{1/2}$ and $2p_{3/2}$ at approximately 724.8 and 711.3 eV were observed, which is consistent with the XRD results. The survey spectra in Figure 3a indicate the presence of nitrogen in both RGO/Fe_3O_4 and NG/Fe_3O_4. For RGO/Fe_3O_4, the introduction of nitrogen is attributed to the reduction agents used in the hydrothermal process, and the nitrogen in NG/Fe_3O_4 results from N_2 plasma treatment. The analysis of the N chemical bonding is shown in Figure 3d, and the N 1s peak can be deconvoluted into three components. The pyridinic and pyrrolic N at 398.2 and 400.1 eV correspond to the N atoms of the π-conjugated system[35,48,49]. The graphitic N at 401.7 eV corresponds to the N atoms

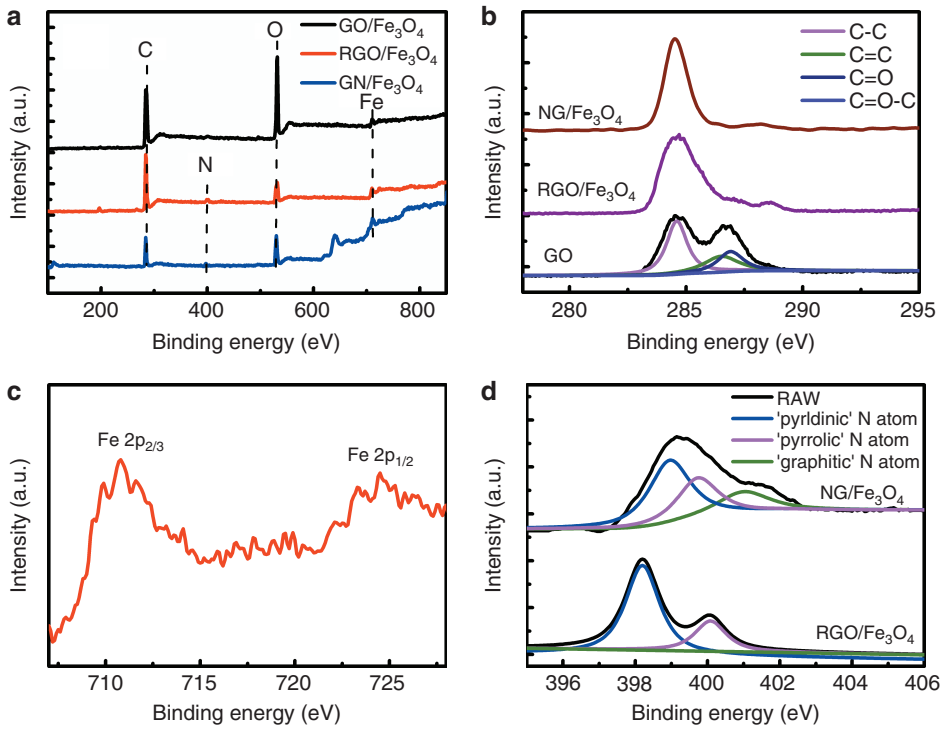

Figure 3 (**a**) XPS surveys of GO/Fe_3O_4, RGO/Fe_3O_4 and NG/Fe_3O_4; (**b**) XPS C 1s spectrum of the GO, RGO/Fe_3O_4 and NG/Fe_3O_4 samples; (**c**) XPS Fe 2p spectrum of the NG/Fe_3O_4 samples; (**d**) XPS N 1s spectrum of the NG/Fe_3O_4 and RGO/Fe_3O_4 samples.

replacing the C atoms inside graphene sheets, which could be observed clearly for NG/Fe_3O_4 but was nearly invisible for RGO/Fe_3O_4, as shown in Figure 3d. The first two types of N atoms located in the π-conjugated system account for most of the N in graphene and contribute one or two p-electrons. The graphitic N atoms can be considered to be threefold coordinated sp^2 N in the hexagonal rings of graphene, which plays an important role in regulating the electronic properties of graphene in electrochemical systems[48,49]. According to our results, the graphitic N doping is difficult to achieve by the hydrothermal method, and plasma treatment is crucial to achieve a high-quality, N-doping, graphene-based aerogel.

A typical three-electrode method was used in this work to investigate the electrochemical behavior. The working electrodes were prepared from RGO/Fe_3O_4 and NG/Fe_3O_4. The CV curves of RGO/Fe_3O_4 and NG/Fe_3O_4 are shown in Figure 4a and 4b. The specific capacitances C (F g^{-1}) can be calculated from the CV curves using the following equation[44]:

$$C = (\int I dv)/(vmV) \quad (1)$$

where V, I, m and v are the potential window (V), the current (A), the mass of the active materials (g) and the scan rate (mV s^{-1}), respectively. Figure 4c summarizes the specific capacitance of the two samples as a function of the scan rate. The NG/Fe_3O_4 electrode reached a maximum of 386 F g^{-1} at 5 mV s^{-1}, which was much higher than that of the RGO/Fe_3O_4 electrode (253.3 F g^{-1}). Due to the *in situ* preparation of the RGO/Fe_3O_4@ Ni-foam electrode, the specific capacitance at 5 mV s^{-1} was 267 F g^{-1}, which was slightly improved compared with that of the RGO/Fe_3O_4 electrode but was still far behind the NG/Fe_3O_4 electrode. The galvanostatic charge – discharge lines of the NG/Fe_3O_4 electrode exhibit an almost symmetric triangular shape (Figure 4d), indicating a high reversibility in the charge and discharge cycle[50–52]. Figure 5a shows the Nyquist plots of the NG/Fe_3O_4 and RGO/Fe_3O_4 electrodes. For both samples, the Nyquist plots consist of two distinct parts: a linear part at low frequency and a semicircle part at high frequency. The two samples exhibit similar plots. In the high-frequency part (inset of Figure 5a), the charge transfer resistance (Rct) was calculated as 0.9 and 0.85 Ω for the NG/Fe_3O_4 and RGO/Fe_3O_4 electrodes, respectively. The bulk electrical conductivity of the NG/Fe_3O_4 aerogel sample was 174 S m^{-1}, three times greater than that of RGO/Fe_3O_4 (55 S m^{-1}). Although the conductive agent (conductive carbon black in this work) was absent in the preparation progress of the NG/Fe_3O_4 electrode, the Rct of the NG/Fe_3O_4 electrode has a similar value to that of the RGO/Fe_3O_4 electrode, which is also lower than in some previous studies[44,53], indicating the excellent conductivity of NG/Fe_3O_4.The NG/Fe_3O_4 electrode shows excellent cycling stability, as shown in Figure 5b, and there is no obvious decrease in capacitance after 1000 cycles, which is crucial for commercial applications of supercapacitors[54–56].

The addition of pseudocapacitor materials is an efficient way to improve the performance of graphene-based supercapacitors. Two very important pseudocapacitor materials are transition metal compounds and conducting polymers. Generally, supercapacitors based on conducting polymers have higher specific capacitance than transition metal compounds; however, their cyclic stability is often poor[57]. Transition metal compounds have improved cyclic stability, but the weaknesses of the transition metal compounds are poor mechanical strength and low electrical conductivity. An efficient strategy to improve supercapacitor performance would be a combination of

doi:10.1038/lsa.2016.130

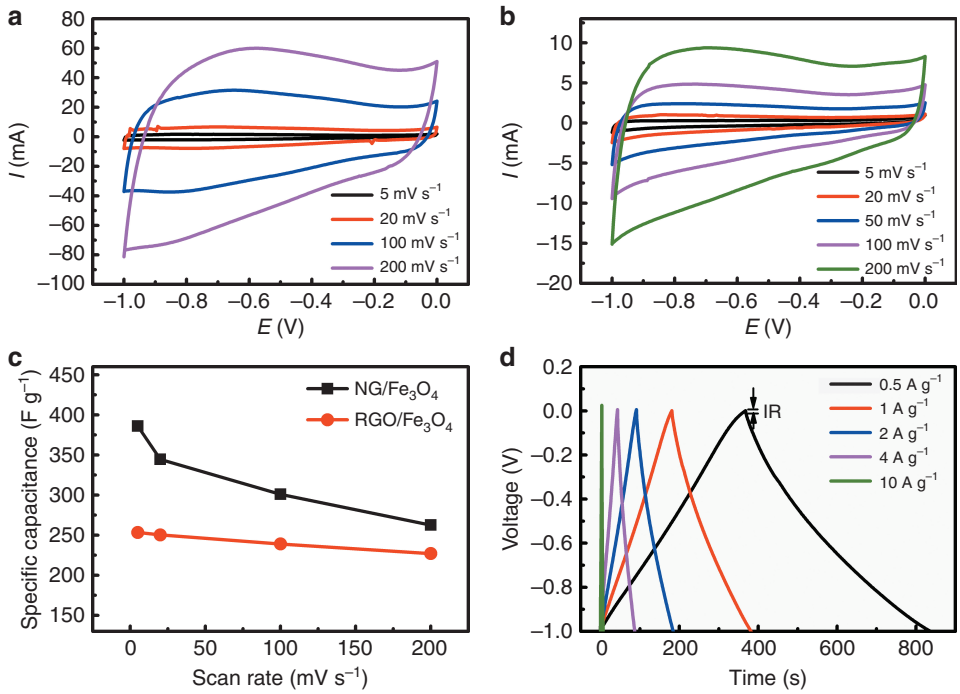

Figure 4 (**a**) CV curves of the RGO/Fe_3O_4 electrode. (**b**) CV curves of the NG/Fe_3O_4 electrode. (**c**) Variation of the specific capacitance against the scan rate for the RGO/Fe_3O_4 and NG/Fe_3O_4 electrodes. (**d**) Galvanostatic charge – discharge curves of the NG/Fe_3O_4 electrode.

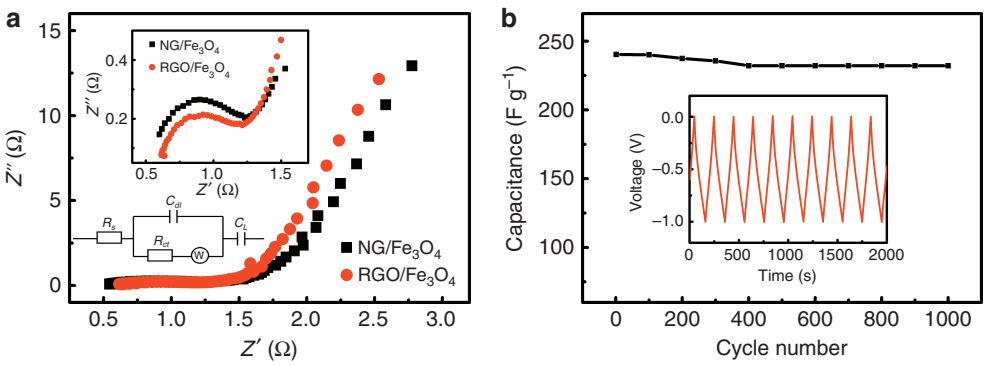

Figure 5 (**a**) EIS of the RGO/Fe_3O_4 and NG/Fe_3O_4 electrodes, with insets showing the high-frequency parts and the equivalent circuit diagram used for fitting the EIS date. (**b**) Cycle performance of the NG/Fe_3O_4 electrode at a current density of 2 A g^{-1}. The inset shows the first 10 cycles of galvanostatic charge – discharge. EIS, electrochemical impedance spectra.

transition metal compounds in highly conductive 3D graphene frameworks. In the present work, we further developed the commonly used hydrothermal method and have shown that plasma-treated NG/Fe_3O_4 would greatly enhance supercapacitor performance. Due to the non-toxicity, easy redox reactions and low cost of Fe_3O_4, it has become a good candidate as a pseudocapacitor material, although its theoretical specific capacitance is lower than that of some other transition metal compounds, such as MnO_2, RuO_2 and V_2O_5[20,58-60]. Table 1 summarizes the performances of supercapacitors prepared with similar 3D systems[20,58,59,61–67]. For 3D graphene aerogels prepared by CVD with Ni-foam and integrated with oxides[58,59,67], they exhibit large specific surface area and low defects, and these aerogels can be used directly without further reduction. However, the CVD methods generally require rigorous conditions, such as high temperature, templates and dangerous gas. Furthermore, the limited output prevents its expansion for industrialization. In the present work, 3D structures were prepared by *in situ* plasma reduction, which is a simple and feasible strategy that can be expanded for large-scale production of nitrogen-doped, graphene-based aerogel, and various active nanomaterials can be incorporated into the 3D hybrid structures. In addition, the present method demonstrates competitive specific capacitance compared with CVD methods.

Compared with other supercapacitors based on Fe_3O_4/RGO structures[61–64], the present NG/Fe_3O_4 shows excellent specific capacitance and charge transfer ability. Because of the intrinsic properties of the materials, the specific capacitance of the NG/Fe_3O_4 electrode is

Table 1 Summary of the capacitive performance of the supercapacitors based on similar structures

Sample	Fabrication method	*Cs* (F g^{-1})	*R* (Ω)	*T*	*C* (%)	Ref
NG/Fe_3O_4	Freeze-drying/plasma reduction and doping	386	0.9	1000	97	Present work
MnO_2/RGO	Dip coating	450	6.5	10 000	90	20
MnO_2/CNT/GE/Ni-foam	CVD	251	1.25	3000	82	58
RuO_2/CNT/GE/Ni-foam	CVD/dip coating	502.7	1.02	8000	106	59
Fe_3O_4/G	2D sandwich-like sheet grown on GO/RGO	349	—	1000	—	61
Fe_3O_4/RGO	Hydrogen reducing	262	—	1000	—	62
Fe_3O_4/RGO	Hydrothermal	220	1.62	3000	—	63
Fe_3O_4/GS	Vacuum filtration/ heat treatment	368	—	1000	—	64
RGO/porous	Electrochemical exfoliation	325	3.6	5000	98	65
3D-RGO	Hydrothermal polymerization/carbonization	225	—	5000	94	66
GE/Ni-foam	CVD	180	0.93	2000	100	67

Abbreviations: *C*, retention rate of C_s after the cycle life test; C_s, specific capacitance; CNT, carbon nanotube; GE, graphene; GS, graphene sheet; *R*, internal resistance obtained from the electrochemical impedance spectra measurements; *T*, cycles of the cycle life test.

still lower than that of MnO_2/RGO and RuO_2/RGO electrodes[20,58,59]. However, the present method is a simple and feasible one compared with the traditional hydrothermal process and CVD method. The active nanomaterials can be further expanded for other compounds of transition metals, such as Co, Ni, Mn, Mo and V. The dip-coating and plasma treatment strategy works well for the 3D NG/Fe_3O_4 system and would also be effective for other compounds of transition metals. The properties of some other materials, such as cobalt oxide and $Ni(OH)_2$, which have 'battery' electrochemical behavior, are not compared[68].

CONCLUSIONS

In conclusion, we have developed a plasma treatment approach to fabricate 3D NG/Fe_3O_4 nanostructures as high-performance supercapacitor electrode materials. During the plasma process, the GO of the GO/Fe_3O_4 materials was reduced and N-doped. The as-prepared NG/Fe_3O_4 electrode exhibited good electrochemical performance, especially high specific capacitance, excellent stability and low charge transfer resistance. As a mature, simple, efficient, low-cost and environmentally friendly method, plasma treatment is a promising process for the preparation and modification of energy storage materials.

ACKNOWLEDGEMENTS

The authors are grateful for funding by the National Natural Science Foundation of China (grant nos. 61322406, 61376020, 11474035 and 61574021).

1 Chen ZP, Ren WC, Gao LB, Liu BL, Pei SF *et al.* Three-dimensional flexible and conductive interconnected graphene networks grown by chemical vapour deposition. *Nat Mater* 2011; **10**: 424–428.
2 Niu ZQ, Chen J, Hng HH, Ma J, Chen XD. A leavening strategy to prepare reduced graphene oxide foams. *Adv Mater* 2012; **24**: 4144–4150.
3 Dai ZG, Xiao XH, Wu Wei, Zhang YP, Liao L *et al.* Plasmon-driven reaction controlled by the number of graphene layers and localized surface plasmon distribution during optical excitation. *Light Sci Appl* 2015; **4**: e342, doi:10.1038/lsa.2015.115.
4 Meng C, Yu SL, Wang HQ, Cao Y, Tong LM *et al.* Graphene-doped polymer nanofibers for low-threshold nonlinear optical waveguiding. *Light Sci Appl* 2015; **4**: e348, doi:10.1038/lsa.2015.121 .
5 Chen JH, Zheng BC, Shao GH, Ge SJ, Xu F *et al.* An all-optical modulator based on a stereo graphene-microfiber structure. *Light Sci Appl* 2015; **4**: e360, doi:10.1038/lsa.2015.133.
6 Xu YX, Sheng KX, Li C, Shi GQ. Self-assembled graphene hydrogel via a one-step hydrothermal process. *ACS Nano* 2010; **4**: 4324–4330.
7 Yin SY, Zhang YY, Kong JH, Zou CJ, Li CM *et al.* Assembly of graphene sheets into hierarchical structures for high-performance energy storage. *ACS Nano* 2011; **5**: 3831–3838.
8 Liu F, Seo TS. A controllable self-assembly method for large-scale synthesis of graphene sponges and free-standing graphene films. *Adv Funct Mater* 2010; **20**: 1930–1936.
9 Maiti UN, Lim J, Lee KE, Lee WJ, Kim SO. Three-dimensional shape engineered interfacial gelation of reduced graphene oxide for high rate large capacity supercapacitors. *Adv Mater* 2014; **26**: 615–619.
10 Xu YX, Lin ZY, Huang XQ, Wang Y, Huang Y *et al.* Functionalized graphene hydrogel-based high-performance supercapacitors. *Adv Mater* 2013; **25**: 5779–5784.
11 Ariga K, Vinu A, Yamauchi Y, Ji QM, Hill JP. Nanoarchitectonics for mesoporous materials. *Bull Chem Soc Jpn* 2012; **85**: 1–32.
12 Li ZX, Barnes JC, Bosoy A, Stoddart JF, Zink JI. Mesoporous silica nanoparticles in biomedical applications. *Chem Soc Rev* 2012; **41**: 2590–2605.
13 Tang FQ, Li LL, Chen D. Mesoporous silica nanoparticles: synthesis, biocompatibility and drug delivery. *Adv Mater* 2012; **24**: 1504–1534.
14 Worsley MA, Pauzauskie PJ, Olson TY, Biener J, Satcher JH *et al.* Synthesis of graphene aerogel with high electrical conductivity. *J Am Chem Soc* 2010; **132**: 14067–14069.
15 Luo JY, Jang HD, Sun T, Xiao L, He Z *et al.* Compression and aggregation-resistant particles of crumpled soft sheets. *ACS Nano* 2011; **5**: 8943–8949.
16 Ji QM, Honma I, Paek SM, Akada M, Hill JP *et al.* Layer-by-layer films of graphene and ionic liquids for highly selective gas sensing. *Angew Chem Int Ed* 2010; **49**: 9737–9739.
17 El-Kady MF, Strong V, Dubin S, Kaner RB. Laser scribing of high-performance and flexible graphene-based electrochemical capacitors. *Science* 2012; **335**: 1326–1330.
18 Wei W, Yang SB, Zhou HX, Lieberwirth I, Feng XL *et al.* 3D graphene foams cross-linked with pre-encapsulated Fe_3O_4 nanospheres for enhanced lithium storage. *Adv Mater* 2013; **25**: 2909–2914.
19 Li C, Shi GQ. Three-dimensional grapheme architectures. *Nanoscale* 2012; **4**: 5549–5563.
20 Ge J, Yao HB, Hu W, Yu XF, Yan YX *et al.* Facile dip coating processed graphene/MnO_2 nanostructured sponges as high performance supercapacitor electrodes. *Nano Energy* 2013; **2**: 505–513.
21 Huang KJ, Wang L, Zhang JZ, Wang LL, Mo YP. One-step preparation of layered molybdenum disulfide/multi-walled carbon nanotube composites for enhanced performance supercapacitor. *Energy* 2014; **67**: 234–240.
22 Augustyn V, Simonbc P, Dunn B. Pseudocapacitive oxide materials for high-rate electrochemical energy storage. *Energy Environ Sci* 2014; **7**: 1597–1614.
23 Shi EZ, Li HB, Xu WJ, Wu ST, Wei JQ *et al.* Improvement of graphene-Si solar cells by embroidering graphene with a carbon nanotube spider-web. *Nano Energy* 2015; **17**: 216–223.
24 Wu SP, Ge RY, Lu MJ, Xu R, Zhang Z. Graphene-based nano-materials for lithium-sulfur battery and sodium-ion battery. *Nano Energy* 2015; **15**: 379–405.
25 Fan ZJ, Yan J, Zhi LJ, Zhang Q, Wei T *et al.* A three-dimensional carbon nanotube/graphene sandwich and its application as electrode in supercapacitors. *Adv Mater* 2010; **22**: 3723–3728.
26 Estevez L, Kelarakis A, Gong QM, Da'as EH, Giannelis EP. Multifunctional graphene/platinum/nafion hybrids via ice templating. *J Am Chem Soc* 2011; **133**: 6122–6125.
27 Vickery JL, Patil AJ, Mann S. Fabrication of graphene-polymer nanocomposites with higher-order three-dimensional architectures. *Adv Mater* 2009; **21**: 2180–2184.
28 Du J, Lai XY, Yang NL, Zhai J, Kisailus D *et al.* Hierarchically ordered macro-mesoporous TiO_2-graphene composite films: improved mass transfer, reduced charge recombination, and their enhanced photocatalytic activities. *ACS Nano* 2011; **5**: 590–596.
29 Cong HP, Ren XC, Wang P, Yu SH. Macroscopic multifunctional graphene-based hydrogels and aerogels by a metal ion induced self-assembly process. *ACS Nano* 2012; **6**: 2693–2703.
30 Tang ZH, Shen SL, Zhuang J, Wang X. Noble-metal-promoted three-dimensional macroassembly of single-layered graphene oxide. *Angew Chem Int Ed* 2010; **49**: 4603–4607.
31 Wang Y, Wu YP, Huang Y, Zhang F, Yang X *et al.* Preventing graphene sheets from restacking for high-capacitance performance. *J Phys Chem C* 2011; **115**: 23192–23197.

32 Bai H, Sheng KX, Zhang PF, Li C, Shi GQ. Graphene oxide/conducting polymer composite hydrogels. *J Mater Chem* 2011; **21**: 18653–18658.
33 Xu YX, Wu QO, Sun YQ, Bai H, Shi GQ. Three-dimensional self-assembly of graphene oxide and DNA into multifunctional hydrogels. *ACS Nano* 2010; **4**: 7358–7362.
34 Chen WF, Li SR, Chen CH, Yan LF. Self-assembly and embedding of nanoparticles by in situ reduced graphene for preparation of a 3D graphene/nanoparticle aerogel. *Adv Mater* 2011; **23**: 5679–5683.
35 Wei DC, Liu YQ, Wang Y, Zhang HL, Huang LP *et al.* Synthesis of N-doped graphene by chemical vapor deposition and its electrical properties. *Nano Lett* 2009; **9**: 1752–1758.
36 Giovannetti G, Khomyakov PA, Brocks G, Karpan VM, Brink JV *et al.* Doping graphene with metal contact. *Phys Rev Lett* 2008; **101**: 026803.
37 Wang Y, Shao YY, Matson DW, Li JH, Lin YH. Nitrogen-doped graphene and its application in electrochemical biosensing. *ACS Nano* 2010; **4**: 1790–1798.
38 Zhou YC, Leng YH, Zhou WJ, Huang JL, Zhao MW *et al.* Sulfur and nitrogen self-doped carbon nanosheets derived from peanut root nodules as high-efficiency non-metal electrocatalyst for hydrogen evolution reaction. *Nano Energy* 2015; **16**: 357–366.
39 Chai LY, Wang JX, Wang HY, Zhang LY, Yu WT *et al.* Porous carbonized graphene-embedded fungus film as an interlayer for superior Li-S batteries. *Nano Energy* 2015; **17**: 224–232.
40 Wang XR, Li XL, Zhang L, Yoon Y, Weber PK *et al.* N-Doping of graphene through electrothermal reactions with ammonia. *Science* 2009; **324**: 768–771.
41 Panchokarla LS, Subrahmanyam KS, Saha SK, Govindaraj A, Krishnamurthy HR *et al.* Synthesis, structure, and properties of boron- and nitrogen-doped graphene. *Adv Mater* 2009; **21**: 4726–4730.
42 Qin Y, Yuan J, Li J, Chen DC, Kong Y *et al.* Crosslinking graphene oxide into robust 3D porous N-doped graphene. *Adv Mater* 2015; **27**: 5171–5175.
43 Lin YC, Lin CY, Chiu PW. Controllable graphene N-doping with ammonia plasma. *Appl Phys Lett* 2010; **96**: 133110.
44 Wu XL, Wen T, Guo HL, Yang SB, Wang XK *et al.* Biomass-derived sponge-like carbonaceous hydrogels and aerogels for supercapacitors. *ACS Nano* 2013; **7**: 3589–3597.
45 Sun XM, Li YD. Colloidal carbon spheres and their core/shell structures with noble-metal nanoparticles. *Angew Chem Int Ed* 2004; **43**: 597–601.
46 Grzyb B, Hildenbrand C, Berthon-Fabry S, Bégin D, Job N *et al.* Functionalisation and chemical characterisation of cellulose-derived carbon aerogels. *Carbon* 2010; **48**: 2297–2307.
47 Wang G, Liu T, Xie XL, Ren ZY, Bai JB *et al.* Structure and electrochemical performance of Fe_3O_4/graphene nanocomposite as anode material for lithium-ion batteries. *Mater Chem Phys* 2011; **128**: 336–340.
48 Wang XB, Liu YQ, Zhu DB, Zhang L, Ma HZ *et al.* Controllable growth, structure and low field emission of well-aligned CN_x nanotubes. *J Phys Chem B* 2002; **106**: 2186–2190.
49 Casanovas J, Ricart JM, Rubio J, Illas F, Jiménez-Mateos JM. Origin of the large N 1s binding energy in X-ray photoelectron spectra of calcined carbonaceous materials. *J Am Chem Soc* 1996; **118**: 8071–8076.
50 Wang HB, Liu ZH, Chen X, Han PX, Dong SM *et al.* Exfoliated graphite nanosheets/carbon nanotubes hybrid materials for superior performance supercapacitors. *J Solid State Electrochem* 2011; **15**: 1179–1184.
51 Lei ZB, Shi FH, Lu L. Incorporation of MnO_2-coated carbon nanotubes between graphene sheets as supercapacitor electrode. *ACS Appl Mater Interfaces* 2012; **4**: 1058–1064.
52 Choi BG, Yang MH, Hong WH, Choi JW, Huh YS. 3D macroporous graphene frameworks for supercapacitors with high energy and power densities. *ACS Nano* 2012; **6**: 4020–4028.
53 Qie L, Chen WM, Xu HH, Xiong XQ, Jiang Y *et al.* Synthesis of functionalized 3D hierarchical porous carbon for high-performance supercapacitors. *Energy Environ Sci* 2013; **6**: 2497–2504.
54 Sun WP, Rui XH, Ulaganathan M, Madhavi S, Yan QY. Few-layered $Ni(OH)_2$ nanosheets for high-performance supercapacitors. *J Power Sources* 2015; **295**: 323–328.
55 He SJ, Chen W. Application of biomass-derived flexible carbon cloth coated with MnO_2 nanosheets in supercapacitors. *J Power Sources* 2015; **294**: 150–158.
56 Lin SY, Zhang XT. Two-dimensional titanium carbide electrode with large mass loading for supercapacitor. *J Power Sources* 2015; **294**: 354–359.
57 He SJ, Chen W. 3D graphene nanomaterials for binder-free supercapacitors: scientific design for enhanced performance. *Nanoscale* 2015; **7**: 6957–6990.
58 Zhu GY, He Z, Chen J, Zhao J, Feng XM *et al.* Highly conductive three-dimensional MnO_2-carbon nanotube-graphene-Ni hybrid foam as a binder-free supercapacitor electrode. *Nanoscale* 2014; **6**: 1079–1085.
59 Wang W, Guo SR, Lee I, Ahmed K, Zhong JB *et al.* Hydrous ruthenium oxide nanoparticles anchored to graphene and carbon nanotube hybrid foam for supercapacitors. *Sci Rep* 2014; **4**: 4452–4460.
60 Shakir I, Ali Z, Bae J, Park J, Kang DJ. Layer by layer assembly of ultrathin V_2O_5 anchored MWCNTs and graphene on textile fabrics for fabrication of high energy density flexible supercapacitor electrodes. *Nanoscale* 2014; **6**: 4125–4130.
61 Qu QT, Yang SB, Feng XL. 2D sandwich-like sheets of iron oxide grown on graphene as high energy anode material for supercapacitors. *Adv Mater* 2011; **23**: 5574–5580.
62 Cheng JP, Shou QL, Wu JS, Liu F, Dravid VP *et al.* Influence of component content on the capacitance of magnetite/reduced graphene oxide composite. *J Electroanal Chem* 2013; **698**: 1–8.
63 Wang QH, Jiao LF, Du HM, Wang YJ, Yuan HT. Fe_3O_4 nanoparticles grown on graphene as advanced electrode materials for supercapacitors. *J Power Sources* 2014; **245**: 101–106.
64 Liu MM, Sun J. *In situ* growth of monodisperse Fe_3O_4 nanoparticles on graphene as flexible paper for supercapacitor. *J Mater Chem A* 2014; **2**: 12068–12074.
65 Jung SM, Mafra DL, Lin CT, Jung HY, Kong J. Controlled porous structures of graphene aerogels and their effect on supercapacitor performance. *Nanoscale* 2015; **7**: 4386–4393.
66 Zhang L, Zhang F, Yang X, Long GK, Wu YP *et al.* Porous 3D graphene-based bulk materials with exceptional high surface area and excellent conductivity for supercapacitors. *Sci Rep* 2013; **3**: 10481–10489.
67 Bo Z, Zhu WG, Ma W, Wen ZH, Shuai XR *et al.* Graphene supercapacitors: vertically oriented graphene bridging active-layer/current-collector interface for ultrahigh rate supercapacitors. *Adv Mater* 2013; **25**: 5798–5806.
68 Thierry B, Daniel B, Jeffrey WL. To be or not to be pseudocapacitive. *J Electrochem Soc* 2015; **162**: A5185–A5189.

This work is licensed under a Creative Commons Attribution 4.0 International License. The images or other third party material in this article are included in the article's Creative Commons license, unless indicated otherwise in the credit line; if the material is not included under the Creative Commons license, users will need to obtain permission from the license holder to reproduce the material. To view a copy of this license, visit http://creativecommons.org/licenses/by/4.0/

© The Author(s) 2016

Supplementary Information for this article can be found on the *Light: Science & Applications*' website (http://www.nature.com/lsa).